

# Exhaustive Symbolic Regression

Deaglan J. Bartlett<sup>1</sup>, Harry Desmond<sup>2</sup>, and Pedro G. Ferreira<sup>3</sup>

**Abstract**—Symbolic Regression (SR) algorithms learn analytic expressions which both accurately fit data and, unlike traditional machine-learning approaches, are highly interpretable. Conventional SR suffers from two fundamental issues which we address in this work. First, since the number of possible equations grows exponentially with complexity, typical SR methods search the space stochastically and hence do not necessarily find the best function. In many cases, the target problems of SR are sufficiently simple that a brute-force approach is not only feasible, but desirable. Second, the criteria used to select the equation which optimally balances accuracy with simplicity have been variable and poorly motivated. To address these issues we introduce a new method for SR – *Exhaustive Symbolic Regression* (ESR) – which systematically and efficiently considers all possible equations and is therefore guaranteed to find not only the true optimum but also a complete function ranking. Utilising the minimum description length principle, we introduce a principled method for combining these preferences into a single objective statistic. To illustrate the power of ESR we apply it to a catalogue of cosmic chronometers and the Pantheon+ sample of supernovae to learn the Hubble rate as a function of redshift, finding  $\sim 40$  functions (out of 5.2 million considered) that fit the data more economically than the Friedmann equation. These low-redshift data therefore do not necessarily prefer a  $\Lambda$ CDM expansion history, and traditional SR algorithms that return only the Pareto-front, even if they found this successfully, would not locate  $\Lambda$ CDM. We make our code and full equation sets publicly available [DOI](#).

**Index Terms**—Symbolic regression, data analysis, minimum description length, model selection, cosmology



## 1 INTRODUCTION

SYMBOLIC Regression (SR) is the umbrella term for machine-learning methods that incorporate the functional form into the search space of regression, enabling optimisation over operators and their ordering as well as the values of numerical parameters. The most popular technique for SR is the Genetic Algorithm (e.g. [1]–[4]), in which a population of equations is evolved through several generations by means of mutations and cross-breeding. By setting an equation’s probability of reproducing to be an increasing function of its fitness (here its accuracy when evaluated on the dataset), the overall fitness of the population rises over time as the equations selected become increasingly suitable for describing the data in question. Other techniques include reinforcement learning [5] and physics-inspired approaches which search for symmetries to simplify the data [6], [7].

Given a set of basis functions, there are an infinite number of ways of combining such operators to produce equations which could describe the data. The aim of SR is not just to fit the data but to be interpretable and hence produce the simplest equations possible. Increasingly com-

plex functions achieve higher accuracy on the dataset but exhibit lower generalisability due to overfitting. Minimising complexity thus becomes a second objective, and optimisation produces a Pareto front of functions which are not surpassed in either objective without the other becoming worse. Models at the knee of the Pareto front are typically selected as exhibiting the optimum tradeoff of accuracy and complexity. Alternatively, more complex models may be explicitly penalised within the fitness function to retain a single-objective problem.

By searching for simple, analytic descriptions of the data, the advantage of SR algorithms over traditional machine learning methods is their interpretability and clear extrapolation behaviour when employed on data outside the range of the training set. A potentially more important, yet more optimistic, goal of SR is to uncover “physical laws” from data, which are necessarily analytic. For example, SR has recently been used to rediscover the laws governing planetary motions from the trajectories of the Sun and the Solar System’s planets and large moons [4].

As such, SR has recently been utilised in the field of astrophysics to find effective prescriptions for the outcomes of complex, non-linear numerical simulations. For example, using SR, it has been found that multiplying the conventional integrated thermal Sunyaev-Zeldovich flux [8],  $Y$ , by  $1 + M_*/M_{\text{gas}}$ , where  $M_*$  and  $M_{\text{gas}}$  are the stellar and gas masses of a cluster, provides a relationship with the halo mass,  $M$ , which is more robust to feedback processes than the traditional  $Y - M$  relation [9]. Delgado et al. [10] use SR to find corrections to the standard halo occupation distribution, which describes the mean number of galaxies with a given set of parameters residing in a dark matter halo. The relations they find are remarkably simple; for example, the fractional correction to the number of satellites is simply  $q' - A$ , where  $A$  is a free parameter and  $q'$  is the

- D.J. Bartlett is with CNRS & Sorbonne Université, Institut d’Astrophysique de Paris (IAP), UMR 7095, 98 bis bd Arago, F-75014 Paris, France.  
Email: deaglan.bartlett@physics.ox.ac.uk
- H. Desmond is with Institute of Cosmology & Gravitation, University of Portsmouth, Dennis Sciamia Building, Portsmouth, PO1 3FX, UK.  
Email: harry.desmond@port.ac.uk
- D.J. Bartlett was with and P.G. Ferreira is with Astrophysics, University of Oxford, Denys Wilkinson Building, Keble Road, Oxford OX1 3RH, UK.

Manuscript received XXXX, YYYY; accepted XXXX, YYYY, date of publication XXXX, YYYY

(Corresponding authors: Deaglan J. Bartlett, Harry Desmond)

Recommended for acceptance by BBBB

Digital Object Identifier no. AAAA

variable used to capture the tidal shear. Using SR to determine an effective description can be particularly useful in other areas of physics; for example, SR has been employed to learn (macroscopic) transport terms required for continuity equations from microscopic-scale numerical simulations [11]. In all of these examples we see that the equations found by the SR are sufficiently simple that one should question whether it is necessary to stochastically search through only a subset of functions at fixed complexity, or whether, to guarantee one has found the optimal solution, one should systematically search through all possible equations.

While state-of-the-art implementations of SR achieve high performance on test-bench problems, they are not infallible [12]. On any given dataset there is a (generally unknown) probability that the algorithm will fail to converge to the optimal solution, or more generally that functions near the Pareto front will not have been considered. We have therefore developed a new algorithm for SR, dubbed *Exhaustive Symbolic Regression* (ESR). ESR explicitly considers every possible combination of operators up to a given complexity of equation, which we define as the number of nodes in the function’s tree representation. By considering all possible equations, ESR is guaranteed to find the best-fitting function at a given complexity, and therefore the true Pareto front.

Since the typical goal of SR is to find trade-off between accuracy and simplicity to obtain the “best” equation for a given dataset, one must define a procedure for combining these competing metrics. Currently, there exists almost as many methods for assessing this balance as there are SR implementations. For example, with PYSR [13], [14] one can select the most accurate equation or the equation from some region of the Pareto front with the maximum score (defined to be the negative first derivative of the logarithm of the loss function with respect to complexity). The former of these clearly has no penalty for overly complicated equations, whereas the score method has little motivation from an information-theoretic perspective. The selection criterion and complexity definition utilised in AIFEYNMAN [6], [7] is better motivated, drawing on the minimum description length principle. However, their final selection criterion does not consider the number of parameters used, and all parameters are penalised in the complexity by an arbitrary number (set by a precision hyperparameter), rather than by considering the constraining power of the data on these parameters. These limitations preclude the combination of accuracy and simplicity into a single objective.

To combat this fundamental issue with current SR algorithms, we develop an implementation of the minimum description length principle to assess functions, which naturally penalises those that are more structurally or parametrically complex, and those whose parameters must be specified more precisely to yield a high accuracy. Statistics such as the one derived in this work could be incorporated into current and future SR implementations to enable a principled, objective conclusion: without such motivation the outputs of SR algorithms are essentially arbitrary.

This paper presents the first iteration of the ESR algorithm in which we consider functions of only one variable (denoted  $x$  throughout) up to complexity 10.

We present the algorithm in detail in Sections 2 and 3 and

apply it to simple test cases to demonstrate its behaviour in Section 4. We compare to traditional SR algorithms and discuss future avenues in Section 5 and conclude in Section 6. We publicly release the results and code (📄).

A forthcoming paper (Desmond, Bartlett & Ferreira, in prep) presents the first detailed and substantially non-trivial application of ESR (to galaxy dynamics).

## 2 FUNCTION GENERATION

In this section we describe how we generate all possible functions at a given complexity and fit the parameters of these functions to data. We then present the generated functions for a typical set of basis functions and discuss the typical behaviour which can be captured by such functions. Of the variant forms for a function at given complexity, we select one to be the “unique equation” representing that subset. While all variants of the same unique equation will give the same maximum likelihood for the data, and thus we need to only optimise the parameters of the unique equations, these variants may provide simpler descriptions of the data in the information theoretic sense that we make precise in Section 3. We therefore retain all variants at this stage. We do not, however, consider any other choices for the numerical parameters unless the likelihood or dataset is changed, in which case the optimisation must be repeated.

To do this, one must have a definition of complexity. By representing the basis functions as nodes, one can represent the functions of interest as trees, and thus a natural definition of complexity is the number of nodes in the tree. We therefore wish to generate all possible expressions from our basis functions that can be represented as a tree with a given number of nodes.

In this section we outline how we achieve this. In Section 2.1 we demonstrate how functions can be represented as trees, which can be stored as lists of operators. We then discuss how we produce all valid equations in Section 2.2 and how duplicates are identified and handled in Section 2.3. The method used to optimise the parameters of the generated equations is outlined in Section 2.4, and we detail the number of functions produced and their properties in Section 2.5.

### 2.1 Tree representation

To begin, we will assert that all operators take a fixed number of arguments. In this paper we will consider three types of operator: binary (e.g.  $+$ ,  $\times$ ,  $\text{pow}$ ), unary (e.g.  $\text{exp}$ ,  $\text{log}$ ,  $\text{square}$ ), or nullary (constants, parameters or variables). When one sees a binary operator in the tree, for example, one knows that this node is either the “root” of the tree or has one “parent” node, and that it has two “child” nodes (the arguments of the function). Hence, one can uniquely reconstruct the tree from a list of operators if one has a rule for traversing the tree, where the length of the list equals the complexity of the function.

As in Petersen et al. [15], the first operator in our list is the “root” node, which we place at the top of the tree. If this operator is binary, we draw two nodes connected to the root, and the second operator in the list is placed on the left hand node. If the operator was unary, we would

$$(\log(x))^{\theta_0} + \exp(\theta_1 x) = [+ , \text{pow}, \text{log}, x, \theta_0, \text{exp}, *, \theta_1, x]$$

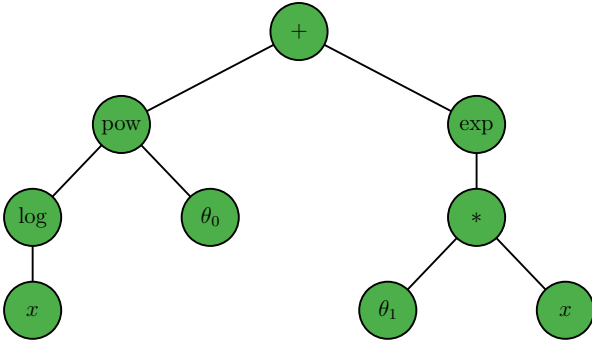


Fig. 1. Representations of the expression  $(\log(x))^{\theta_0} + \exp(\theta_1 x)$  as a tree and as a list of operators. One can generate the tree from the list using the traversal rule outlined in Section 2.1. The mapping from the list to the function is unique, however a given equation does not necessarily have a unique tree representation. For example, this equation could also be represented as  $[+, \text{exp}, *, \theta_1, x, \text{pow}, \text{log}, x, \theta_0]$  or  $[+, \text{exp}, *, x, \theta_1, \text{pow}, \text{log}, x, \theta_0]$ . One could also interchange the parameters  $\theta_0$  and  $\theta_1$ , since these are parameters to be fitted to the data and thus the two expressions would be equivalent after optimising these parameters.

only draw one node connected to the root, as the second operator labels this node. We continue traversing the tree down and to the left as far as possible, until we reach a nullary operator. We then go back up the tree to find the next node which has an unlabelled child on its right, and place the next operator in the list there. As an example, in Fig. 1 we give one of the tree representations of the expression  $(\log(x))^{\theta_0} + \exp(\theta_1 x)$ , written both as a tree and as the corresponding list of operators.

We note two important properties of this representation which we exploit in the ESR algorithm. First, the mapping between the list and the tree is bijective, hence we choose the list representation throughout. Therefore, our task is to find all possible lists of a given length which produce valid functions. Second, a given function may have multiple tree representations and hence there is a redundancy to this notation. For efficiency in fitting parameters of the functions to data, an ESR algorithm should be able to identify these duplicates.

## 2.2 Generating valid trees

The number of equations grows exponentially as one increases complexity; for  $n$  basis functions there are  $n^k$  possible lists for functions comprised of  $k$  nodes. However, not all of these will produce valid functions. For example, neither the list  $[\theta_0, +, x]$  nor  $[+, +, x]$  produce valid functions. Fortunately, one does not have to check all  $n^k$  lists to see if they can represent functions, since e.g.  $[*, x, \text{exp}]$  and  $[*, x, \text{square}]$  fail for the same reason: both  $\text{exp}$  and  $\text{square}$  are unary operators.

Our first task is to identify all possible tree structures (without being concerned about the node labels) and how these can be represented as lists. We produce all possible lists of length  $k$  made from combinations of '0', '1' and '2', where 0, 1 and 2 are placeholders for nullary, unary and binary operators, respectively. We then attempt to convert these lists into trees using the traversal rule outlined in

Section 2.1, and only keep those lists which produce valid trees. For example, for  $k = 4$  there are only four valid graph structures:  $[1,1,1,0]$ ,  $[1,2,0,0]$ ,  $[2,0,1,0]$  and  $[2,1,0,0]$  out of a possible  $3^4 = 81$  combinations of '0', '1' and '2'. The generation of all valid functions is trivial once we have all valid tree structures: one simply considers all possible ways of decorating the nodes with the correct type of operator from the list of basis functions.

In fact, we do not need to consider all  $3^k$  trees. Since we know that (for  $k > 1$ ) the final node must be nullary, whereas the first node cannot be, we now only need to check the validity of  $2 \times 3^{k-2}$  lists if  $k > 2$ , whereas there is only one valid tree shape for  $k = 1, 2$ . In general this will be much smaller than  $n^k$ . Moreover, one does not need to consider all  $2 \times 3^{k-2}$  lists, since if a list of length  $\kappa < k$  nodes forms a valid function, this list cannot form the start of a list for a function of complexity  $k$ , so we can immediately rule out such cases.

## 2.3 Duplicate checking and simplifications

Now that we have all possible equations at a given complexity for a given set of basis functions, we could stop there and fit the parameters of each equation to the data. However, this would be inefficient as there exist duplicate equations, so it is sensible to identify the unique equations and only optimise their parameters. We therefore check for the following patterns which give duplicate equations:

- *Tree reordering*: The trees  $[+, \theta_0, x]$  and  $[+, x, \theta_0]$  give the same equation, as we have simply swapped the left and right nodes of the '+' operator. This highlights a redundancy in the tree notation. We identify all equations which are equivalent but whose operators have a different ordering in the tree.
- *Simplifications*: We also search for functions which are mathematically equivalent but expressed in different ways. For example, one may generate both the factorised and expanded version of a polynomial. We use the SYMPY [16] package to convert our function trees into symbolic expressions to help identify these cases.
- *Parameter permutations*: The functions  $\theta_0 + \theta_1 x$  and  $\theta_1 + \theta_0 x$  are distinct for given parameters  $\theta_0$  and  $\theta_1$ , however we wish to fit these parameters to the data and thus these will return identical expressions once optimised, so should be identified as equivalent. This is a special case of reparameterisation invariance.
- *Reparameterisation invariance*: Suppose we have two functions  $\exp(\theta_0) \times x$  and  $\text{square}(\theta_0) \times x$ . When optimised, these will give different values of  $\theta_0$ , however the coefficient of  $x$  in the function will be the same in both cases. Therefore, these should be considered duplicate equations, and only one of these needs to be fitted to the data.
- *Parameter combinations*: If parameters only appear in our equations as combinations of other parameters (e.g.  $\theta_0 + \theta_1 + x$ ), then these functions can be expressed as trees of lower complexity ( $\theta_0 + x$  in our example). Since the more complicated version of this function will perform worse with respect to all sensible metrics which balance simplicity with accuracy,

we discard the expression with two parameters in favour of the equation with one.

Typically, one would not include integers in the set of basis function. However, some equations are more naturally expressed if one chooses to include these; for example, one would write  $2x$  instead of  $x + x$ . We therefore additionally search for sums of equivalent expressions in the generated equations and find tree representations where these are written as a constant multiplied by the repeated sub-expression. Similarly, when evaluating logarithms and exponentials, one may prefer to write  $\exp(4x)$  to square (square( $\exp(x)$ )). Our duplicate checker also finds such equations (and the logarithmic equivalents) and generates new trees containing multiplication by constants. By design, these equations are not unique, however these may be favourable representations when functions are compared in Section 3.

## 2.4 Numerical parameter optimisation

Functions up to complexity 10 contain 0-4 free parameters  $\theta$ . The next step is to optimise these parameters to maximise the likelihood,  $\mathcal{L}$ , of the data given the function, for which we use the BFGS algorithm. For functions with 1 or 2 parameters we work in  $\log_{10}(|\theta|)$ , optimising separately for  $\theta < 0$  and  $\theta > 0$  and taking the better result. This allows the algorithm to efficiently search a larger range in the parameters and can improve convergence. For functions of 3 or 4 parameters we work directly in  $\theta$  to avoid the proliferation of separate positive and negative branches.

Any individual run of the BFGS optimiser may converge to a local likelihood maximum, or fail to converge at all. We therefore repeat the optimisation  $N_{\text{iter}}$  times with different random starting positions, selecting the best result. To reduce runtime for functions that are simple to optimise, we end early if  $N_{\text{conv}}$  iterations of the optimiser give a result within  $\Delta \log \mathcal{L} = 0.5$  of the best solution found so far. The count is reset to 0 if any iteration achieves a result better than the best solution so far found by  $\Delta \log \mathcal{L} = 2$ , which we deem to be a different local maximum. We select random starting positions from a uniform distribution within  $[0,3]$  in cases where  $\theta$  itself is optimised, and  $\pm[1,10^3]$  where  $\log(\theta)$  is optimised. For the examples given in Section 4 we choose  $N_{\text{iter}} = 30$  and  $N_{\text{conv}} = 5$ , and have found these hyperparameter choices to result in robust optimisation in the great majority of cases, but they may be readily altered by the user in our public code release.

## 2.5 Generated Equations

To quantify the number of functions one should consider and the impact of the simplification steps employed, we generate all possible equations for the set of basis functions  $\{x, a, \text{inv}, +, -, \times, \div, \text{pow}\}$  up to complexity 10.<sup>1</sup> The number of equations with a given number of free parameters at each complexity are shown in Fig. 2. We show separately the

1. Note that several of these operators may be constructed from others, e.g.  $-$  from  $+$  and  $a$  and  $\text{inv}$  from  $\text{pow}$  and  $a$ . Including them explicitly reduces the complexity of functions containing them, increasing the diversity of equations up to a given complexity.

number of unique equations, which are the only ones whose parameters we need to optimise, and the total number.

It is immediately clear that the simplification procedures implemented in the ESR algorithm dramatically reduces the number of functions one needs to consider. The naïve estimate of  $n^k$  functions for  $n$  basis functions and  $k$  nodes would suggest that one should consider approximately 168 million functions up to complexity 10. We find only 5.2 million of these are valid trees, and 134,234 of these are unique, which is a factor of 1250 smaller than the original estimate. Moreover, we only need to optimise functions which contain parameters, and thus we must run our optimisation procedure on only 119,861 functions (1400 times fewer than the original estimate). Not only is this a feasible number of functions, but this second step is embarrassingly parallelisable as each function is optimised in isolation.

The functions generated when complexity equals 1 or 2 are extremely straightforward; at complexity 1, one can only generate a constant or the function  $y = x$ , and at complexity 2 one can either have a unary operator acting on  $x$  or on a constant, the latter of which yields another constant. However, by complexity 3 one already has useful physical equations. For example, the function  $\theta_0/x$ , which represents the Newtonian gravitational potential for a point mass orbiting a spherically symmetric body, can be expressed as  $[\div, \theta_0, x]$ . At complexity 5, one can fit both a straight line ( $[+, \times, \theta_0, x, \theta_1]$ ) and a power law ( $[\times, \theta_0, \text{pow}, x, \theta_1]$ ). As will be discussed further in Section 4, at complexity 7 one can add a constant to a power law and thus generate a Friedmann equation for a universe consisting of a cosmological constant and a perfect fluid. A Navarro-Frenk-White (NFW) profile [17] with a free outer slope ( $[\div, \theta_0, \times, x, \text{pow}, +, x, \theta_1, \theta_2]$ ) is produced at complexity 9, and thus at this complexity one can generate functions which have two power law limits. A Cauchy-Lorentz (Breit-Wigner)-like distribution is also produced at this complexity ( $[\div, \theta_0, +, \text{pow}, -, x, \theta_1, \theta_2, \theta_3]$ ), allowing one to fit resonances. Of course, with a different set of basis functions one would find alternative equations at these complexities; however, even with our simple basis set, it is interesting to see how many useful physical expressions expressions can be generated by complexity 10.

Up to and including complexity 10, one does not need to optimise more than four parameters. It is straightforward to show that, if one wants an equation which depends on the input variable  $x$ , then at complexity  $k$  any function containing nullary, unary and binary operators cannot contain more than  $\lfloor (k-1)/2 \rfloor$  parameters.

The ESR algorithm is split into two distinct stages; first, one calculates all possible functions and attempts to remove duplicates, and in the second stage one fits these to the data. If one does not wish to change the basis functions, then the first step does not need to be rerun when one changes dataset or problem considered. Although we make the functions used in this work publicly available [18] so one may not need to repeat the function generation, for reference, we note that generating all equations and identifying duplicates took 25 seconds at complexity 7 when run with 24 cores, with a maximum memory usage of 137MB.

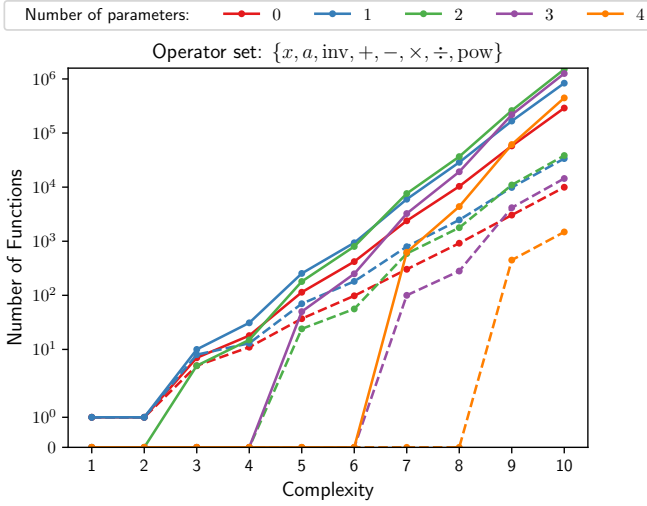


Fig. 2. The number of trial functions containing  $p$  parameters at each complexity constructed from the basis functions  $\{x, a, \text{inv}, +, -, \times, \div, \text{pow}\}$ . The solid lines indicate the *total* number of equations, and the dashed lines are the number of *unique* equations identified in the ESR search. Although the number of functions grows exponentially with complexity, identifying duplicates dramatically reduces the number of equations one needs to consider. At complexity 10, we see that, once duplicates are removed, an exhaustive search only requires one to consider  $\mathcal{O}(10^4 - 10^5)$  functions.

### 3 MODEL SELECTION BY MINIMUM DESCRIPTION LENGTH

We now require a metric for quantifying the “goodness” of a given equation. The simplest choice is of course the likelihood,  $\mathcal{L}$ , itself, which describes the accuracy with which the equation reproduces the data. This is however prone to overfitting, since more complex equations will tend to match the data better while generalising worse to unseen data. With reduced  $\chi^2$  inappropriate due to the neglect of the normalisation of the Gaussian likelihood (which is essential if one has errors on  $x$ ) and difficulties for correlated data and nonlinear functions [19], common statistics for tackling overfitting include the Akaike (AIC), Bayesian (BIC) and Deviance (DIC) information criteria, which combine the maximum-likelihood value with a term that depends on the number of free parameters, and the Bayesian evidence which assesses the proximity of parameters’ posteriors to their priors. We do not adopt a Bayesian perspective here as we consider only the maximum-likelihood parameter values. Aside from the specific assumptions that go into the information criteria, their major issue is that they account for *parametric* but not *functional* complexity, making them suitable for numerical but not symbolic regression. Two functions with an equal number of free parameters will have the same AIC, BIC and DIC regardless of the operator set used in the functions and the number of times operators appear.

The *minimum description length principle* (MDL) provides a natural framework in which to solve this problem [20]. MDL posits that the best functional representation of a dataset is the one that compresses it most, so that the fewest units of information are needed to communicate the data with the help of the function. This is best understood by

means of a two-part code for conveying the data: first one encodes the functional form, then one encodes the residuals of the data points around the function’s expectation:

$$L(D) = L(H) + L(D|H), \quad (1)$$

where  $L$  here denotes codelength (not to be confused with likelihood  $\mathcal{L}$ ),  $H$  is the functional hypothesis and  $D$  the data. Roughly speaking,  $L(D|H)$  is an accuracy term describing how well the function fits the data, and  $L(H)$  penalises more complex hypotheses. On the two extremes are *i*) a function which fits the dataset perfectly so that  $L(D|H) = 0$  but  $L(H)$  is probably very large, and *ii*) the simplest hypothesis “0” which has  $L(H) = 0$  and  $L(D|H) = L(D)$  probably very large. The best equation, minimising  $L(D)$ , will generically be somewhere in the middle. MDL is reviewed in [21]–[23].

Under the Shannon–Fano coding scheme [24], the optimal encoding of the residuals has  $L(D|H) = -\log(\mathcal{L}(D|\hat{\theta}))$ , where  $\theta$  are the function’s free parameters and a hat denotes the maximum-likelihood points (derived in Section 2.4). We note that changing the units of the observable will change  $L(D|H)$  by an additive constant, however, since this constant is the same for all models applied to the same data, this is unimportant in the context of model comparison. The description length of the model,  $L(H)$ , is composed of a functional part and a parameter part. For the functional part, if the number of nodes in the function’s tree is  $k$  then we must transmit  $k$  blocks of information, and each one must then specify which operator is appearing in that block. If the operator set has size  $n$  (that is, the function is composed of  $n$  unique operators), that requires  $\log(n)$  nats per chunk, so that specifying the functional form in total requires  $k \log(n)$  units of information. We use the nat as our unit of information, so all logs are base- $e$ .

Parameters are included in the operator set, but unlike the other operators we must also specify their values, which requires further information. Assuming that all parameters are real numbers (i.e. no simplification for integers or rationals), then the  $i^{\text{th}}$  parameter requires  $\log(|\theta_i|/\Delta_i) + \log(2)$  nats, where  $\Delta_i$  is the precision to which it is specified and the final bit ( $\log(2)$  nats) specifies the sign.<sup>2</sup> We use a codelength  $\log(c)$  for any constant  $c$  that has arisen in the function simplification process (Section 2.3), corresponding to a natural number representation.<sup>3</sup> We note that this represents a lower bound on the number of nats required to transfer  $\theta_i$  or  $c$ , since, to be decipherable, the codewords used must form a prefix set. Various optimal schemes are possible, which require a code length  $L(c)$  to transfer the natural number  $c$  such that  $\log(c) < L(c) < \log(c) + R(c)$ , where  $R(c)/\log(c) \rightarrow 0$  as  $c \rightarrow \infty$  [25], but differ in their specific values for a given  $c$ . Since all optimal solutions have  $\log(c)$  as their leading order term [25], we choose to ignore higher order corrections to remain agnostic to the exact prefix code utilised. As such, this term penalises parameters slightly less than it would need to in practice.

<sup>2</sup> In practice one would have to round up to an integer number of information units, but this is unnecessary for our purposes.

<sup>3</sup> Negation must therefore be included in the operator list should any constant be negative.



The total description length is then

$$\begin{aligned} L(D) &\equiv L(D|H) + L(H) \\ &= -\log(\mathcal{L}(\hat{\theta})) + k \log(n) + p \log(2) + \sum_j \log(c_j) \\ &\quad + \sum_i^p \log(|\hat{\theta}_i|/\Delta_i), \end{aligned} \quad (2)$$

where  $p$  is the total number of free parameters. The only degrees of freedom here are the  $\Delta_i$ . In keeping with the MDL principle, we choose these by minimising the right hand side of Eq. (2) [20]. Increasing  $\Delta_i$  (i.e. specifying the parameter to lower precision) reduces the parameter code-length  $\log(|\hat{\theta}_i|/\Delta_i)$  but increases the first, log-likelihood term because the communicated, rounded value is likely to be further from the maximum-likelihood value. Rounding to the nearest  $\Delta_i$  gives  $\theta_i$  a uniform probability in  $[\hat{\theta}_i - \Delta_i/2, \hat{\theta}_i + \Delta_i/2]$ . We find what loss this incurs by Taylor-expanding  $-\log(\mathcal{L})$  around its minimum:

$$-\log(\mathcal{L}(\hat{\theta} + \mathbf{d})) \approx -\log(\mathcal{L}(\hat{\theta})) + \frac{1}{2} \mathbf{d}^T \mathbf{I} \mathbf{d}, \quad (3)$$

where  $d_i$  is a uniform random variable in  $[-\Delta_i/2, \Delta_i/2]$  and  $\mathbf{I}$  is the Fisher information matrix. This provides an expected contribution to the description length

$$L(\Delta) = \frac{1}{2} \sum_{ij} \langle l_{ij} d_i d_j \rangle - \sum_i \log(\Delta_i), \quad (4)$$

where the 2<sup>nd</sup> term on the right hand side comes from the denominator of the final term in Eq. (2) (the only part that depends on  $\Delta_i$ ). Since the  $d_i$  are independent of one another,  $\langle l_{ij} d_i d_j \rangle = l_{ii} \langle d_i^2 \rangle \delta_{ij}$  and we see that only the diagonal elements of the Fisher matrix contribute and the parameters' contributions decouple. Using that  $\langle d_i^2 \rangle = \Delta_i^2/12$ , we have

$$L(\Delta_i) = \frac{1}{24} l_{ii} \Delta_i^2 - \log(\Delta_i), \quad (5)$$

which is minimised for

$$\Delta_i = \left( \frac{12}{l_{ii}} \right)^{1/2}. \quad (6)$$

We choose this  $\Delta_i$  such that the expectation value of  $L(\Delta)$  is minimised [20], [26], but note that an alternative common choice is to minimise the maximum of this quantity [25]. This difference – corresponding to minimisation of an average or worse-case description length over possible datasets – is not important for our purposes. This implies a total description length

$$\begin{aligned} L(D) &= -\log(\mathcal{L}(\hat{\theta})) + k \log(n) - \frac{p}{2} \log(3) \\ &\quad + \sum_i^p \left( \frac{1}{2} \log(l_{ii}) + \log(|\hat{\theta}_i|) \right), \end{aligned} \quad (7)$$

which is the quantity we seek to minimise over the function set.<sup>4</sup>

4. Note that we optimise the parameter vector purely for the likelihood. This is in general not the same as optimising it for the code length due to the  $\frac{1}{2} \log(l_{ii}) + \log(|\hat{\theta}_i|)$  term. That alternative procedure is more computationally expensive as the full parameter code length would have to be calculated for each step of the optimiser.

There may arise cases in which  $|\hat{\theta}_i|/\Delta_i < 1$  so that the maximum-likelihood value of a parameter cannot be distinguished from 0 within the tolerance given by Eq. (6). Following Rissanen [20], in this case we set the parameter to 0, recalculate the likelihood and reduce  $p$  by 1. Since this occurs precisely in cases where the parameter is poorly distinguished from 0 anyway, this generically has little effect on  $L(D)$ .

When we assess the tradeoff between simplicity and accuracy, the true tree representation will be important. Instead of simply discarding all duplicates found in Section 2.3, we determine the function which maps the parameters in the unique function,  $\varphi$ , to those in the original equation,  $\theta$ . To calculate  $L(D)$ , we must evaluate the Fisher information matrix at the maximum likelihood point

$$\mathbf{I}_{ij}^{(\theta)} \equiv - \left. \frac{\partial^2 \log \mathcal{L}}{\partial \theta_i \partial \theta_j} \right|_{\theta=\hat{\theta}}, \quad (8)$$

but will have calculated

$$\mathbf{I}_{ij}^{(\varphi)} \equiv - \left. \frac{\partial^2 \log \mathcal{L}}{\partial \varphi_i \partial \varphi_j} \right|_{\varphi=\hat{\varphi}}. \quad (9)$$

We therefore calculate the Jacobian for our transformations

$$\mathbf{J}_{ij} \equiv \frac{\partial \theta_i}{\partial \varphi_j}, \quad (10)$$

so that we can transform the Fisher matrix as

$$\mathbf{I}^{(\theta)} = \left( \mathbf{J}^{-1} \right)^T \mathbf{I}^{(\varphi)} \mathbf{J}^{-1}. \quad (11)$$

We end this section by noting that MDL is not wedded to the notion that there exists a “true” hypothesis which it is the job of the model selection algorithm to find. Rather, MDL formalises Occam’s razor by seeking to find the most economical description of the data, which is typically the one that generalises the best. Thus, it is naturally expected that MDL will prefer less simple but more accurate functions the more data is available: the simplicity terms in Eq. (7) become less important compared to the likelihood.

## 4 CASE STUDIES

As an example of an application of the ESR algorithm, in this section we attempt to determine the expansion rate of the Universe at low redshift,  $z$ , by reconstructing the square of Hubble parameter,  $H(z)$ . In particular, we wish to learn the function  $y(x \equiv 1+z) \equiv (H(z))^2$ . According to the standard cosmological model ( $\Lambda$ CDM), well after matter-radiation equality and assuming spatial flatness,  $y(x)$  takes the simple form

$$y_{\Lambda\text{CDM}}(x) = \theta_0 + \theta_1 x^3, \quad (12)$$

which, for the basis functions described in Section 2.5, is a complexity 7 function:  $[+, \theta_0, \times, \theta_1, \text{pow}, x, 3]$ .

We apply the ESR algorithm using this basis separately to a sample of  $H(z)$  measurements from cosmic chronometers and to measurements of the distances to supernovae of known redshift to determine whether Eq. (12) is preferred by the data, or whether there exists alternative best-fitting functions. We note that applying SR to observed cosmological data has previously been achieved using Genetic

Algorithms [27]–[34], however this is the first application of the ESR algorithm to this problem. Moreover, unlike previous work, through our model selection via the MDL, we naturally include penalties in a principled manner for unnecessarily complex equations, and by considering all possible equations we do not rely on arbitrary stopping criteria. We outline the observational data used and the likelihoods employed in Section 4.1, and the results are presented and discussed in Section 4.2. In Section 4.3 we analyse mock cosmic chronometer data generated according to  $\Lambda$ CDM, to determine the requirements for the MDL principle to select this as the best model.

## 4.1 Observational data

### 4.1.1 Cosmic chronometers

For a Friedmann–Lemaître–Robertson–Walker metric, the Hubble parameter is related to redshift,  $z$ , and cosmic time,  $t$  as

$$H(z) = -\frac{1}{1+z} \frac{dz}{dt}, \quad (13)$$

which is independent of the constituents or curvature of such a universe. The key concept for cosmic chronometer studies, introduced by Jimenez & Loeb [35], is to measure this quantity by approximating  $dz/dt \approx \delta z/\delta t$ , where  $\delta z$  and  $\delta t$  are small but finite differences between different objects. One can determine  $\delta t$  by identifying stellar populations which evolve passively since these act as standard clocks, and  $\delta z$  is a directly measurable quantity.

In this section we use a sample of 32 cosmic chronometer measurements of  $H(z)$  from the literature [36]–[43], compiled by Moresco *et al.* [44]. We treat each of these measurements as independent and compare to our prediction,  $H(z) = \sqrt{y}$ , by assuming a Gaussian likelihood,

$$\log \mathcal{L} = -\frac{1}{2} \sum_i \left( \frac{(H(z_i^o) - H_i^o)^2}{\sigma_i^2} + \log(2\pi\sigma_i^2) \right), \quad (14)$$

where  $\{H_i^o\}$  are the set of observed Hubble rates at redshifts  $\{z_i^o\}$ , each of which has an associated uncertainty  $\sigma_i$ . To remain fully consistent, as discussed in Moresco *et al.* [45], there should be off-diagonal correlations in the likelihood due to modelling assumptions. For simplicity, we will ignore these terms, since our focus here is the application of the ESR algorithm and not cosmic chronometer modelling.

### 4.1.2 Type Ia Supernovae

Type Ia supernovae were the first objects to provide evidence of an expanding Universe [46], [47], and have thus been used extensively over the last few decades to constrain parameters of  $\Lambda$ CDM and its extensions. These objects act as standardisable candles; by combining the observed amplitude of their lightcurves with parameters describing the lightcurve width and colour, and correcting for biases relating to selection and the supernova’s host, one can measure the distance moduli,  $\mu_i^o$ , to these objects, after calibrating against a lower rung of the distance ladder, for example using Cepheids [48], [49]. In this work we utilise the Pantheon+ sample of supernovae [50] alongside the Cepheid distances provided by the SH0ES collaboration [51]. We make use of the publicly available (non-diagonal)

covariance matrix,  $\Sigma$ , produced as part of the Pantheon+ cosmological analysis [52].

To convert the Hubble parameter we are learning,  $H(z) = \sqrt{y}$ , to a distance modulus, we will assume a flat universe. The luminosity distance,  $d_L$ , to a supernova at redshift  $z$  is then

$$d_L(z) = (1+z) \int_0^z \frac{c dz'}{H(z')}, \quad (15)$$

where  $c$  is the speed of light, and this can then be converted to the distance modulus as

$$\mu(z) = 5 \log_{10} \left( \frac{d_L(z)}{10 \text{ pc}} \right). \quad (16)$$

This is then compared to the observed supernova data using a Gaussian likelihood

$$\log \mathcal{L} = -\frac{1}{2} (\boldsymbol{\mu}(z^o) - \boldsymbol{\mu}^o)^T \boldsymbol{\Sigma}^{-1} (\boldsymbol{\mu}(z^o) - \boldsymbol{\mu}^o) - \frac{1}{2} \log(\det(2\pi\boldsymbol{\Sigma})), \quad (17)$$

where  $\boldsymbol{\mu}^o$  and  $\boldsymbol{\mu}(z^o)$  are vectors describing the set of  $\mu^o, \mu(z^o)$  for a given supernova. Since  $\boldsymbol{\Sigma}$  is independent of  $y(x)$ , we do not include the final term in our optimisation as this adds an arbitrary constant to  $\log \mathcal{L}$ , and thus to  $L(D)$ .

## 4.2 Results

We run the ESR algorithm up to complexity 10 separately for the cosmic chronometer and Pantheon+ samples using the basis functions  $\{x, a, \text{inv}, +, -, \times, \div, \text{pow}\}$ , and tabulate the resulting best-fit equations in Tables 1 and 2, respectively. In both cases, we observe that the top five functions – ranked according to their description lengths – contain only one or two parameters, since functions with more parameters require more information to specify their values and they require trees of higher complexity. For reference, in these tables we also give the first Friedmann-like equations for  $\Lambda$ CDM (Eq. (12)) and universes with a cosmological constant and single fluid with an unknown equation of state parameter,

$$y_{\text{fluid}}(x) = \theta_0 + \theta_1 x^{\theta_2}, \quad (18)$$

which we infer. We find that the solution with a free exponent is approximately  $\Lambda$ CDM for both datasets, since  $\theta_2 \approx 3$ . For both datasets we find that Eq. (18) is not preferred by the data, but ranks in the top 100 functions, whereas  $\Lambda$ CDM performs better, and is in the top 40 functions. The  $\Lambda$ CDM equation ranks slightly higher for the Pantheon+ data owing to the increased constraining power of the data: the change in  $\log \mathcal{L}$  for the Pantheon data between Eq. (18) and the MDL function is smaller than for cosmic chronometers. Since this function was generated from the multiplication of three  $x$ ’s in its tree, its complexity is given as 9, as opposed to 7, which would be the case if it were formed from  $\text{pow}(x, 3)$ . If we replace the complexity 9 variant by the complexity 7 one, then the description length of the  $\Lambda$ CDM function marginally decreases, increasing the function’s ranking to 38<sup>th</sup> and 34<sup>th</sup> for the cosmic chronometer and Pantheon+ data, respectively.

Given that we find that a two-component universe is not the most economical description of the data, one may wonder whether a single-component universe provides a

better fit. Indeed, the highest ranked function for the cosmic chronometer data is proportional to the square of  $1 + z$ . This would correspond to a universe consisting exclusively of curvature, however a more appropriate interpretation is that this exponent falls between the values of dark matter (a cubic in  $1 + z$ ) and dark energy (a constant). Similarly, we find that a single component universe,  $y = \theta_0 x^{\theta_1}$ , is the 11<sup>th</sup> highest-ranked function for the Pantheon+ data, with  $\theta_1 = 1.42$ . Again, this exponent is presumably capturing an “average” contribution of the two terms in Eq. (18), but it provides a worse fit by a change in log-likelihood of  $\Delta \log \mathcal{L} = 4.4$ . Interestingly, although containing just a single parameter, we find that a de Sitter universe ( $y = \theta_0$ ) is severely disfavoured by the data; this expansion history ranks 10,058<sup>th</sup> for the cosmic chronometer data and our optimiser fails to find a value of  $\theta_0$  which fits the Pantheon+ sample.

We see that Eq. (18) has a better accuracy (smaller  $-\log \mathcal{L}$ ) than any of the top-5 functions, when ranked by description length. If instead we order *all* functions by log-likelihood, one finds that Eq. (18) actually performs worse; it is the 829<sup>th</sup> and 202<sup>nd</sup> most accurate function for the cosmic chronometer and Pantheon+ data, respectively. The pure  $\Lambda$ CDM expression (Eq. (12)) is ranked even lower; it could not have performed better as it is a special case of Eq. (18). We note that an appropriately-tuned non-exhaustive search which only saves the Pareto front (e.g. AIFEYNMAN [6], [7] or PYSR [13], [14]) would not have found the Friedmann equation as it is not the best fitting function at its complexity. This calls into question whether such probabilistic techniques can be used to find physical laws given limited and imperfect data—unless, of course,  $\Lambda$ CDM is not the true cosmological model.

When one assesses equations according to the likelihood, the five best functions have complexities of either 9 or 10. As one could anticipate, by making functions arbitrarily complex one can improve the fit, however selecting functions according the MDL gives a principled and unambiguous way of determining what complexity of expression is warranted by the data. This can be observed in Fig. 3, where we plot the Pareto fronts of the cosmic chronometer and Pantheon+ data, comparing both the likelihood and description lengths. As one increases complexity, the maximum-likelihood plateaus to become approximately constant, whereas the description length shows a well-defined minimum at a complexity of 5 for both datasets. By collapsing the Pareto front into a single number (the description length), the task of choosing the best function becomes well-defined.

To gain intuition as to why equations which are not Friedmann-like are preferred, in Figs. 4 and 5 we plot the 150 functions with the smallest description lengths alongside the data they are fitted to, and show the residuals with respect to  $\Lambda$ CDM. Almost all functions are effectively indistinguishable for  $z \lesssim 1$ , where the majority of the data is. To understand this, let us first recast Eq. (12) into a more familiar form,

$$\begin{aligned} y_{\Lambda\text{CDM}}(x) &= H_0^2 \left( \Omega_{m0} (1+z)^3 + 1 - \Omega_{m0} \right) \\ &= H_0^2 \left( 1 + 3\Omega_{m0}z + 3\Omega_{m0}z^2 + \Omega_{m0}z^3 \right). \end{aligned} \quad (19)$$

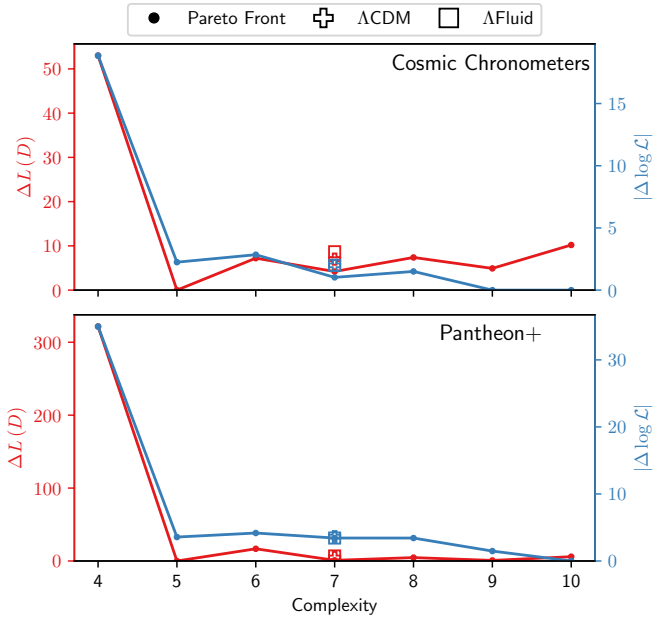


Fig. 3. Pareto front of functions generated with the ESR algorithm, compared to the cosmic chronometer (upper) and Pantheon+ (lower) data. Complexity is defined as the number of nodes in the tree representation of the function, and we show the best-fitting functions according to the change in the description length,  $L$ , and the likelihood,  $\mathcal{L}$ , relative to the corresponding minima. For comparison, we also plot the best-fit  $\Lambda$ CDM solutions as pluses and a more general Friedmann equation (Eq. (18)) with squares. If assessing functions by the likelihood, it is unclear which complexity to choose, whereas according to the MDL prescription, the choice according to the  $L$  is unambiguous; one should pick the minimum at complexity 5.

If we now expand the highest ranked function from the Pantheon+ data about  $z = 0$ ,

$$y(x) = \theta_0 x^x = \theta_0 \left( 1 + z + z^2 + \frac{1}{2}z^3 + \mathcal{O}(z^4) \right), \quad (20)$$

one sees that, since  $\Omega_{m0} = 0.315 \pm 0.007 \approx 1/3$  when inferred using the cosmic microwave background [53], the Taylor series for the  $\Lambda$ CDM and best-fitting function are approximately equal up to and including second order, if one identifies  $\theta_0 = H_0^2$ . It is perhaps, therefore, merely a coincidence that a one-parameter function can fit the local expansion rate, owing to dark matter comprising approximately one third of the present-day energy budget of the Universe and having an equation of state parameter  $w = 0$ .

At redshifts  $z \gtrsim 1$ , we see that the predicted Hubble rate and distance moduli diverge rapidly for the different functions, due to the lack of data in this regime. By having an analytic expression, one can easily identify how these equations will diverge. One could therefore combine this analysis with higher-redshift probes to more tightly constrain the true Hubble rate, since we will no longer be in a regime where the Taylor expansion above is valid, and thus the functions identified in this work will have very different predictions.

### 4.3 ESR on mock data

We have observed that current cosmic chronometer and supernovae data are not sufficiently constraining to prefer  $\Lambda$ CDM over other expansion histories with smaller



Rank	$y(x) / \text{km}^2\text{s}^{-2}\text{Mpc}^{-2}$	Complexity	Parameters			Codelength			
			$\theta_0$	$\theta_1$	$\theta_2$	Residuals <sup>1</sup>	Function <sup>2</sup>	Parameter <sup>3</sup>	Total
1	$\theta_0 x^2$	5	3883.44	-	-	8.36	5.49	2.53	16.39
2	$ \theta_0 ^{x^{\theta_1}}$	5	3982.43	0.22	-	7.97	5.49	5.24	18.70
3	$\theta_0  \theta_1 ^{-x}$	5	1414.43	0.31	-	7.57	6.93	5.58	20.08
4	$\theta_0 x^{\theta_1}$	5	3834.51	2.03	-	8.35	6.93	5.08	20.36
5	$x^2(\theta_0 + x)$	7	3881.85	-	-	8.36	9.70	2.53	20.60
⋮	⋮	⋮	⋮	⋮	⋮	⋮	⋮	⋮	⋮
39	$\theta_0 + \theta_1 x^3$	9	3164.02	1481.71	-	7.28	12.48	3.76	23.51
⋮	⋮	⋮	⋮	⋮	⋮	⋮	⋮	⋮	⋮
84	$\theta_0 + \theta_1 x^{\theta_2}$	7	3322.96	1374.97	3.08	7.27	11.27	6.52	25.06

<sup>1</sup>  $-\log \mathcal{L}(\hat{\theta})$      
<sup>2</sup>  $k \log(n) + \sum_j \log(c_j)$      
<sup>3</sup>  $-\frac{p}{2} \log(3) + \sum_i^p (\frac{1}{2} \log(I_{ii}) + \log(|\hat{\theta}_i|))$

TABLE 1

Highest ranked functions for  $y(x \equiv 1+z) = (H(z))^2$  inferred from cosmic chronometers using the ESR algorithm. The functions are ordered by their description length,  $L(D)$ , and columns 7-9 show give the terms that are summed to obtain this;  $\mathcal{L}$  is the likelihood, the function can be expressed as a tree with  $k$  nodes containing  $n$  different functions, and there are  $p$  parameters in each function. In the columns 4-6 we give the maximum likelihood values of the parameters of each function. For reference, in the final rows we show the first appearances of a Friedmann equation for a  $\Lambda$ CDM universe or a universe containing a cosmological constant and one perfect fluid. Although the parameters for the Friedmann equation match the expectation of concordance  $\Lambda$ CDM, we see that this model is severely penalised by the description length principle, due to the larger functional and parametric complexities. We note that a complexity 7 version of  $\Lambda$ CDM exists, but cannot be found with the current ESR method due to the integer parameter. This variant would be the 38<sup>th</sup> best function according to the MDL principle.

Rank	$y(x) / \text{km}^2\text{s}^{-2}\text{Mpc}^{-2}$	Complexity	Parameters			Codelength			
			$\theta_0$	$\theta_1$	$\theta_2$	Residuals <sup>1</sup>	Function <sup>2</sup>	Parameter <sup>3</sup>	Total
1	$\theta_0 x^x$	5	5345.02	-	-	706.18	6.93	5.11	718.22
2	$ \theta_0 ^{x^{\theta_1}}$	9	5280.11	0.16	-	705.11	5.49	8.41	719.01
3	$\theta_0  \theta_1 ^{-x}$	5	1694.95	0.32	-	701.79	6.93	10.33	719.05
4	$\theta_0 x^{x^{\theta_1}}$	7	5378.69	0.78	-	702.45	9.70	6.98	719.13
5	$ \theta_0 ^{ \theta_1 ^x}$	5	1898.47	1.14	-	701.88	5.49	12.64	720.02
⋮	⋮	⋮	⋮	⋮	⋮	⋮	⋮	⋮	⋮
37	$\theta_0 + \theta_1 x^3$	9	3591.09	1773.63	-	701.85	12.48	8.81	723.13
⋮	⋮	⋮	⋮	⋮	⋮	⋮	⋮	⋮	⋮
96	$\theta_0 + \theta_1 x^{\theta_2}$	7	3280.83	2069.32	2.73	701.64	11.27	12.19	725.10

<sup>1</sup>  $-\log \mathcal{L}(\hat{\theta})$      
<sup>2</sup>  $k \log(n) + \sum_j \log(c_j)$      
<sup>3</sup>  $-\frac{p}{2} \log(3) + \sum_i^p (\frac{1}{2} \log(I_{ii}) + \log(|\hat{\theta}_i|))$

TABLE 2

Same as Table 1, but for the Pantheon+ supernovae data. Again we see that the Friedmann equation is not the optimal fit to the data, although the difference in description length is less severe than for cosmic chronometers, suggesting that the increased constraining power of these data compensate for the extra parameters. As in Table 1, the complexity 7 variant of  $\Lambda$ CDM would rank marginally higher than the complexity 9 one found by ESR, and would be the 34<sup>th</sup> best function. Although we see that Eq. (18) has a larger  $\log \mathcal{L}$  than any of the top-5 functions, we find that there are 201 functions which perform better than this equation when ranked by likelihood.

functional and parametric complexities. In this section we investigate what one would require in order to recover  $\Lambda$ CDM from a cosmic chronometer dataset by analysing mock catalogues.

We begin by drawing  $N_{cc} = 32,000$  redshifts randomly from the range used in Section 4.1.1 (corresponding to a dataset which is 100 times larger than used here), drawing from a uniform distribution in  $\log(1+z)$ . For each redshift, we compute the “true” Hubble expansion rate using Eq. (12) and assuming the Planck 2018 cosmology [53]. To convert this to an “observed” Hubble parameter, we assume that all measurements have the same fractional uncertainty,  $\sigma_H/H$ , and draw these observations from a Gaussian with this width and a mean corresponding to the “true” value. Since the mean fractional uncertainty of the data used in Section 4.1.1 is approximately 20 per cent, we consider four different cases  $\sigma_H/H \in \{0.01, 0.05, 0.10, 0.20\}$  to investigate the effect of improved precision. We then run the ESR algorithm on these data and rank the functions according to the MDL principle.

Once we have run the analysis at fixed  $N_{cc}$ , we wish to convert our results to arbitrary  $N_{cc}$ . Assuming that one obtains the same parameters if one changed  $N_{cc}$ , the only terms that dependent on  $N_{cc}$  in Eq. (7) are those containing  $\log \mathcal{L}$  and  $I_{ii}$ . Both of these variables scale linearly with  $N_{cc}$ , allowing for a trivial transformation. Note that this introduces a term  $p/2 \log N_{cc}$  into the description length, which is reminiscent of one of the terms in the BIC.

For cases where  $\Lambda$ CDM ranks as the highest function, we compute the difference in description length between Eq. (12) and the second best function. Otherwise, we compute the difference between  $\Lambda$ CDM and the highest ranked function. We plot our findings as a function of  $N_{cc}$  for different  $\sigma_H/H$  in Fig. 6, where all points above zero are cases where we would find  $\Lambda$ CDM as the best fitting function. We indicate cases where  $\Lambda$ CDM does not lie in the top two functions by dashed lines.

We find that with current observational uncertainties, one would require  $\sim 10^3$  measurements of  $H$  in this redshift range to have sufficient constraining power for  $\Lambda$ CDM to be

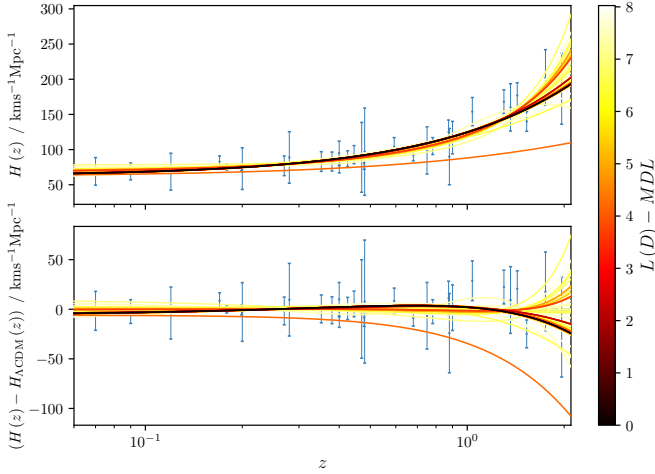


Fig. 4. Hubble parameter,  $H$ , as a function of redshift,  $z$ , learned using the ESR algorithm from cosmic chronometer data (blue points). In the bottom panel we subtract the best-fit  $\Lambda$ CDM prediction. We plot the top 150 functions up to complexity 10, ranked and coloured by their description length,  $L(D)$ , relative to the minimum, MDL. The expansion rate is moderately constrained at low redshift – where most measurements are – but the fits diverge quickly when extrapolated to higher redshifts.

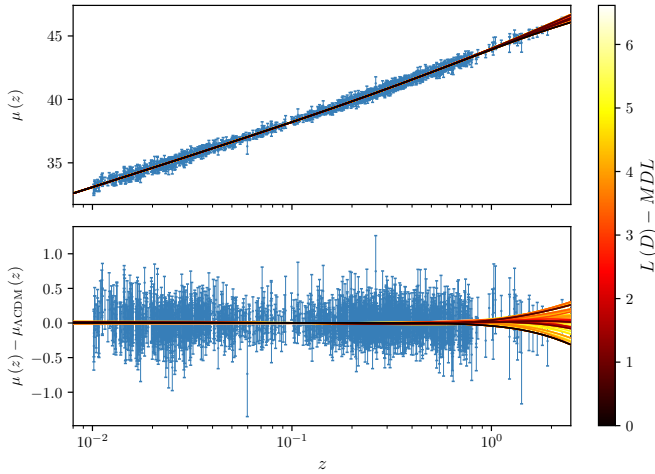


Fig. 5. Distance moduli,  $\mu$ , to Type Ia supernovae in the Pantheon+ catalogue (blue points) as a function of redshift,  $z$ . We plot the 150 highest ranked functions up to complexity 10 inferred using the ESR algorithm and in the lower panel we plot the residuals relative to the best-fit  $\Lambda$ CDM prediction. For  $z < 1$  we see that all functions give very similar expansion histories, but the predicted distance moduli at higher redshifts vary dramatically depending on the chosen function.

the best function. It is therefore no surprise that Eq. (12) performed so poorly on the observed data, where we only have 32 data points. However, if one could reduce the observational uncertainties by a factor of two, then one only requires a few hundred cosmic chronometers for  $\Lambda$ CDM to be recovered. The forecast is even more promising if one could measure  $H$  to within 1 or 5 per cent, since in both cases we see that  $\Lambda$ CDM has the MDL, even if one had only ten cosmic chronometers. These findings therefore suggest that reducing the observational uncertainties on cosmic chronometer measurements is more important than increasing the sample size if one wishes to discriminate

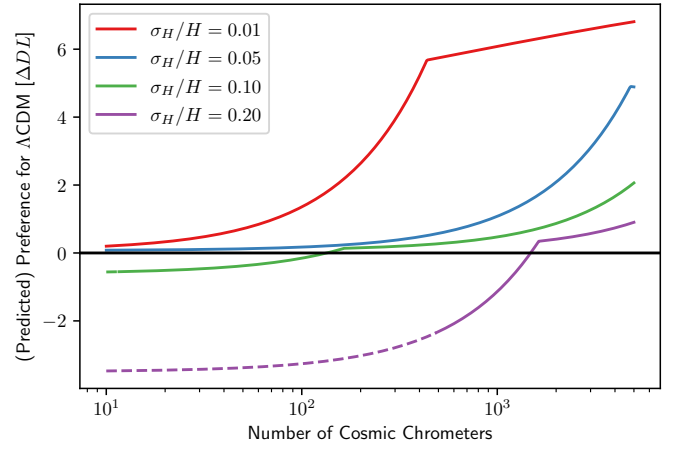


Fig. 6. Change in description length between a  $\Lambda$ CDM expansion history and the highest-ranked non- $\Lambda$ CDM function when applied to mock  $\Lambda$ CDM data as a function of number of cosmic chronometers. Any point greater than zero finds  $\Lambda$ CDM to be the best function and dashed lines indicate analyses where  $\Lambda$ CDM is not in the top two functions. We run the analysis assuming different fractional errors,  $\sigma_H/H$ , on measurements of the Hubble parameter,  $H$ , which for the observed data used in this work is approximately 0.2. One would need over  $10^3$  cosmic chronometers to have enough constraining power with that precision to discover  $\Lambda$ CDM, but this decreases rapidly as the precision improves.

between different expansion histories.

## 5 DISCUSSION

### 5.1 Comparison to traditional SR algorithms

The ESR algorithm systematically searches through all possible equations which can be generated from a given set of basis functions and represented by trees with a fixed number of nodes. This is in contrast to traditional SR methods which, due to the exponential scaling of the number of functions with increasing complexity, do not consider all possible equations but rather attempt to search stochastically through the space of functions. In many applications, since a key goal of SR is interpretability, one often does not want to produce a function with too high complexity, making an exhaustive search of function space feasible. This can be justified by the MDL principle for realistically sized datasets such as we have considered here. Indeed, if one found that a dataset could not be fitted by a simple expression, then one would likely resort to more traditional numerical machine-learning methods, obviating the need for SR at all.

For reference, the correction to the Sunyaev-Zeldovich flux ( $1 + M_*/M_{\text{gas}}$ ) given in Section 1 is a complexity 5 function ( $[1, +, \div, M_*, M_{\text{gas}}]$ ) and the function relevant to the halo occupation distribution ( $q' - A$ ) is only complexity 3 ( $[-, q', A]$ ). These functions are therefore well within the regime for which an exhaustive approach is feasible, and hence the ESR algorithm (were it available at the time) would have provided a more complete solution.

In the unlikely event that one did desire a symbolic expression with high complexity, then one would have to utilise one of these probabilistic methods. However, these methods have a generally unknown probability of failure (not finding the true optimal function in a reasonable

amount of time) that is an unknown function of their hyperparameters, and thus it is important to be able to benchmark these algorithms. By calculating the truth at low complexity, ESR allows the user to evaluate different stochastic methods on their dataset; if the SR algorithm cannot find the true MDL function or Pareto front at low complexity, results at higher complexity are unlikely to be trustworthy. Similarly, once one has chosen a SR algorithm, the results of applying ESR to the data could be useful in hyperparameter optimisation or in initialising a Genetic Algorithm with a starting population of well-fitting functions.

Usually one only discusses the optimal solution or set of Pareto-optimal solutions when considering SR, as this is what traditional SR algorithms are designed to find. Although, in principle, a Genetic Algorithm can provide the full population which it has found and its evolutionary history, common implementations (e.g. PYSR) discard functions which do not lie on the Pareto front. A clear advantage of ESR is the ability to find all functions and their corresponding likelihoods and description lengths. Not only does this allow us to quantify the uncertainty on our prediction in a rigorous and complete way – particularly useful when extrapolating beyond the range of the training set – but we can now propagate uncertainties on the functional form of equations alongside the uncertainties on their parameters when making new predictions. This can be achieved by performing functional integrals, weighting each function by the description length.

On a practical note, the ESR algorithm is naturally a two-step process. We first generate all possible equations at a given complexity, and then we perform the embarrassingly parallel procedure of fitting the parameters to the data. In our implementation, it is trivial to change the likelihood function for this second step, whereas in many SR implementations, since the loss appears many times in the algorithm, it is more difficult to add a custom loss function as one has to hack the backend. The default loss functions in such algorithms is often equivalent to a Gaussian likelihood with a diagonal covariance matrix. In this work we used both a diagonal (Section 4.1.1) and non-diagonal (Section 4.1.2) covariance matrix with a Gaussian likelihood, and in Desmond *et al.* (in prep) we demonstrate how to use more complicated likelihoods, for example by propagating errors on the independent variable  $x$ .

We reiterate that, for our case studies, the equations given in Tables 1 and 2 do not necessarily give the “true” cosmological expansion rate, but are merely the most economical descriptions of the data. Having an exponent of  $1+z$  may be theoretically unfavourable, however by treating all equations equally, the ESR algorithm essentially assumes a flat prior in function space, whereby any equation is an equally probable candidate function. In reality, this may not be the case, and one may want to investigate the impact on different priors on function space, e.g. by applying theoretical priors. In post-processing. The advantage of ESR over traditional algorithms is that, given the ESR algorithm generates and fits all possible equations, one only needs to run the optimisation once; one can easily reweight or remove equations according to different criteria without having to rerun the equation search or parameter optimisation.

In Section 3 we derived an expression (Eq. (7)) from

the description length (Eq. (2)) of a model which naturally combines the accuracy with the parametric and structural complexity of a function into a single summary, which one should optimise to determine which equation is preferred by the data. This statistic incorporates the features one would expect should be in such a criterion: models with lower accuracy, more parameters and more nodes are all punished. Although other SR codes tend to consider a subset of these features in their selection procedure, these are often combined in an ad-hoc manner which make the choice of optimum arbitrary. For example, PYSR considers the derivative of the logarithm of the loss with respect to the complexity; however Eq. (7) suggests differentiating with respect to the logarithm of complexity is more appropriate. As such, it is imperative that well-motivated criteria such as Eq. (7) should be incorporated into traditional SR methods. We note that an attempt to apply the MDL principle has been considered in the AIFEYNMAN package [6], [7], however this did not include all the terms in Eq. (7), or combine the accuracy and simplicity terms to produce an overall description length. In addition, the description lengths of real numbers used in AIFEYNMAN are calculated with an unmotivated parameter precision,  $\Delta_i$ , which greatly penalises real numbers relative to integers or rationals and yields essentially arbitrary values of  $L(D)$ . The MDL principle stands alone from the function generation part of ESR as a model selection algorithm.

## 5.2 Future directions

In this first demonstration of the ESR algorithm, for simplicity, we focused on univariate functions. In many applications, however, one wishes to consider multivariate functions. Although not implemented in the code released with this paper, this extension is conceptually straightforward: when decorating valid tree structures in Section 2.2, one must consider an additional nullary operator for each variable, which will increase the number of functions at a given complexity. To prevent the number of considered variables growing too large, as with other SR algorithms, it may be desirable to first determine which variables are most important through a feature importance analysis with numerical machine learning regressor. One could also consider adding ternary or other higher order  $n$ -ary operators to the set of basis functions, which will require a slightly modified tree traversal rule.

For the case studies chosen in this work, we found that the equations with the MDL have a complexity of 5, and thus we ran our analysis up to and including complexity 10, considering  $5.2 \times 10^6$  functions. As previously discussed, many previous applications of SR also require similar complexity functions, however, in general, one may want to consider higher complexity functions. Since the optimisation procedure is embarrassingly parallel, the main constraint on reaching higher complexities is the function generation process and, in particular, the task of finding duplicates. In the current ESR implementation we have used the SYMPY package to perform many algebraic manipulations and substitutions, however associating a SYMPY function to each equation requires a large amount of memory once one exceeds  $\mathcal{O}(10^6)$  functions. The ESR algorithm is

not tied to this package, and we only use a small subset of its capabilities. Therefore, future implementations of the ESR algorithm may require a simpler, custom symbolic manipulation package to be developed to reduce the memory requirements.

We generated equations in Section 2 utilising tree representations of functions, which can be stored as lists of nodes if one has an appropriate traversal rule. This is an efficient way of generating all equations and we were able to remove 97 per cent of possible lists by considering the topology of trees, making an exhaustive search feasible. However, we find that only up to 26 per cent of the remaining functions are unique. One may therefore wonder whether there is a more economic notation one could exploit with fewer redundancies. Moreover, if one could design a representation with a degree of continuity between operators which have been considered as discrete in this work, one could use fewer basis functions and thus reduce the number of functions to optimise.

In our current search, when we optimise parameters we do not attempt to preferentially find integers or rational numbers over floats. Since such parameters could be encoded with fewer nats than floats, there could exist functions with shorter description lengths than the ones we consider. Our algorithm is therefore exhaustive if considering all functions given a basis set and parameters which are floats, however future work should extend this to parameters which are integers or rational numbers. Note that we capture some of these cases in Section 2.3 by combining e.g.  $x + x$  to form  $2x$  (we also have a “zero-snap” in setting  $\theta_i$  to 0 where  $|\theta_i|/\Delta_i < 1$ ). This process would be unnecessary if one could “snap” floating-point parameters to integers as these equations would naturally appear as functions are generated and compared to data. The Fisher matrix calculated as part of the parameter code length provides a natural way to do this by determining which integers or rationals are close enough to the best-fit float not to degrade the likelihood significantly. One may also wish to prioritise certain irrational numbers which commonly appear in physics (e.g.  $\pi$ ,  $e$  or  $\sqrt{2}$ ), e.g. by defining corresponding custom nullary operators.

Our approach has privileged no class of function, which may be thought of as a uniform prior over functional parameter space (given the predefined operator set). However, it may be possible to exploit symmetries in functions to reduce the description length, or to prefer Hamiltonian or Lagrangian systems. This would favour equations more likely to be found in physics and improve convergence on datasets possessing such features. It may also be possible to endow the function space with a continuity metric by treating equations as solutions of second-order ODEs. While weakly restricting the types of function that could be produced, this would effectively replace functions by the numerical coefficients of the ODE and hence open the door for numerical regression techniques such as gradient descent to explore the space.

Finally, in this work we have only considered the maximum likelihood values of parameters. Although Eq. (7) contains a term related to the Fisher matrix, and thus is related to the uncertainty on the parameters, it would be preferable to consider a more Bayesian approach. Presumably this

would involve using the Bayesian evidence instead of the maximum likelihood in Eq. (7), and thus would marginalise over the uncertainties in the parameters, however we leave it to future work for a more careful analysis. Obtaining the uncertainties on parameters is essential for performing the functional integrals discussed in Section 5.1, as one needs to integrate both over the structural form and the parameters of all equations. One would then also be able to visualise how the uncertainties on these parameters compare to the variations in functional form, since the lines shown in Figs. 4 and 5 would become a posterior for each equation. In Desmond et al. (in prep) we show how explicit Bayesian inference using the lowest description length functions may be used to determine the posterior predictive distributions of physically interesting quantities and hence evaluate the probabilities of competing classes of models.

## 6 CONCLUSION

Symbolic Regression (SR) is a class of inherently interpretable machine-learning methods which learn the analytic expressions that accurately describe data. The conventional approach to this problem involves a stochastic search through parameter space, through e.g. Genetic Algorithms, reinforcement learning or by searching for symmetries in the data, to produce a Pareto-front of viable solutions which balance simplicity with accuracy. Such techniques have a generally unknown probability of failing to obtain the best solution, and little effort has gone into comparing the objectives of simplicity and accuracy to obtain the optimal equation.

In this work we have introduced a novel approach to SR – *Exhaustive Symbolic Regression* (ESR) – which aims to address both of these issues. First, motivated by the relative simplicity of the functions which tend to be selected by SR algorithms, we eliminate the risk of failing to obtain the optimal solution by explicitly considering all possible functions at a given complexity (defined as the number of nodes in the tree representation of a function). Although this problem scales exponentially with complexity, by considering the topology of valid trees and applying simplification procedures to identify duplicate functions, we find that we can reduce the number of functions one needs to fit to the data to a feasible number, which is a factor of  $\sim 1400$  smaller than the naïve expectation. Second, we derive a statistic (Eq. (7)) which combines the likelihood and Fisher matrix with the parametric and structural complexities of a function into a single number describing the amount of information that must be communicated to specify the data with the help of the function. The minimum description length principle asserts that the function minimising this number provides the optimal description of the data. In this way, we collapse the Pareto front into a single summary and thus remove the ambiguity associated with function selection in dual-objective SR algorithms (although of course the full Pareto front may be considered if desired).

As a demonstration of our method, we reconstruct the (square of the) Hubble parameter as a function of redshift from both cosmic chronometers and the Pantheon+ sample of Type Ia supernovae. Interestingly, we find that neither

dataset selects the Friedmann equation as the optimal function, although it does appear in the top 40 of the  $5.2 \times 10^6$  functions considered up to complexity 10. By considering mock- $\Lambda$ CDM data, we find that one would either need to reduce the uncertainties on the cosmic chronometer data by a factor of  $\sim 4$  or increase the sample size by a factor of  $\sim 30$  to have sufficient constraining power for  $\Lambda$ CDM (if it is the correct model) to be rank the highest. These functions all have very similar behaviour for redshifts below one, but deviate wildly above this. We leave it to future work to combine these low-redshift measurements with other data to determine whether  $\Lambda$ CDM is preferred when analysed over a larger range of cosmic time, or in conjunction with other low-redshift probes such as Baryonic Acoustic Oscillations. Furthermore, since the Friedmann equation is not the most accurate function found at its complexity, SR methods which do not save equations away from the Pareto front would not have discovered concordance cosmology even if they had produced the Friedmann equation.

We publicly release our code and the equations generated in this work at [G](#) and [18]. Although we considered one set of basis functions in our analysis, this can be trivially modified to generate the appropriate function set for a given analysis. For example, in our forthcoming paper (Desmond *et al.*, in prep) we apply our method to learn the functional form of the Radial Acceleration Relation of galaxy dynamics, and, motivated by previous fitting formulae, add square, exp and  $\sqrt{\cdot}$  to our basis set. The equations generated in that paper are also made publicly available [18].

Automated discovery of symbolic expressions from data provides easily understood and readily usable descriptions of complex physical processes, and can even discover fundamental physical laws. It is therefore imperative that the model generation and selection algorithms of SR score equations in a rigorous and well-motivated way. By meeting this challenge, the ESR framework improves the prospects for SR to become a key method of data analysis.

## DATA AVAILABILITY

We make available the ESR code [G](#) and function sets generated in this work [18]. The cosmic chronometer data used in Section 4.1.1 can be found in Table 1 of Moresco *et al.* [44]. The supernova data described in Section 4.1.2 was taken from the publicly released Pantheon+ catalogue [G](#). Other data may be shared on request to the corresponding authors.

## ACKNOWLEDGEMENTS

We thank David Bacon, Andrei Constantin, Miles Cranmer, Mario Figueiredo, Gianluca Gregori, Thomas Harvey, Jens Jasche, Mark Kotanchek, Andre Lukas, Benjamin Wandelt and Tariq Yasin for useful inputs and discussion. We thank Jonathan Patterson for smoothly running the Glamdring Cluster hosted by the University of Oxford, where most of the data processing was performed.

DJB is supported by the Simons Collaboration on “Learning the Universe” and was supported by STFC and Oriol College, Oxford. HD is supported by a Royal Society University Research Fellowship (grant no. 211046). PGF acknowledges support from European Research Council

Grant No: 693024 and the Beecroft Trust. This project has received funding from the European Research Council (ERC) under the European Union’s Horizon 2020 research and innovation programme (grant agreement No 693024).

This work used the DiRAC Complexity and DiRAC@Durham facilities, operated by the University of Leicester IT Services and Institute for Computational Cosmology, which form part of the STFC DiRAC HPC Facility ([www.dirac.ac.uk](http://www.dirac.ac.uk)). This equipment is funded by BIS National E-Infrastructure capital grants ST/K000373/1, ST/P002293/1, ST/R002371/1 and ST/S002502/1, STFC DiRAC Operations grant ST/K0003259/1, and Durham University and STFC operations grant ST/R000832/1. DiRAC is part of the National E-Infrastructure.

This work made use of the ASTROPY [54], MATPLOTLIB [55], MPI4PY [56], MPMATH [57], NETWORKX [58], NUMDIFFTOOLS [59], NUMPY [60], PANDAS [61], [62], SCIPY [63] and SYMPY [16] packages.

For the purpose of open access, the authors have applied a Creative Commons Attribution (CC BY) licence to any Author Accepted Manuscript version arising.

## REFERENCES

- [1] A. M. Turing, “I.—COMPUTING MACHINERY AND INTELLIGENCE,” *Mind*, vol. LIX, no. 236, pp. 433–460, 10 1950. [Online]. Available: <https://doi.org/10.1093/mind/LIX.236.433>
- [2] E. David, *Genetic Algorithms in Search, Optimization and Machine Learning*. Addison-Wesley, 1989.
- [3] R. Haupt and S. Haupt, *Practical genetic algorithms*, 2nd ed. Wiley, 2004.
- [4] P. Lemos, N. Jeffrey, M. Cranmer, S. Ho, and P. Battaglia, “Rediscovering orbital mechanics with machine learning,” *arXiv e-prints*, p. arXiv:2202.02306, Feb. 2022.
- [5] R. Sutton and A. Barto, *Reinforcement Learning, second edition: An Introduction*, ser. Adaptive Computation and Machine Learning series. MIT Press, 2018. [Online]. Available: <https://books.google.co.uk/books?id=sWV0DwAAQBAJ>
- [6] S.-M. Udrescu and M. Tegmark, “AI Feynman: A physics-inspired method for symbolic regression,” *Science Advances*, vol. 6, no. 16, p. eaay2631, Apr. 2020.
- [7] S.-M. Udrescu, A. Tan, J. Feng, O. Neto, T. Wu, and M. Tegmark, “AI Feynman 2.0: Pareto-optimal symbolic regression exploiting graph modularity,” *arXiv e-prints*, p. arXiv:2006.10782, Jun. 2020.
- [8] R. A. Sunyaev and Y. B. Zeldovich, “The Observations of Relic Radiation as a Test of the Nature of X-Ray Radiation from the Clusters of Galaxies,” *Comments on Astrophysics and Space Physics*, vol. 4, p. 173, Nov. 1972.
- [9] D. Wadekar, L. Thiele, J. C. Hill, S. Pandey, F. Villaescusa-Navarro, D. N. Spergel, M. Cranmer, D. Nagai, D. Anglés-Alcázar, S. Ho, and L. Hernquist, “The SZ flux-mass ( $Y$ - $M$ ) relation at low halo masses: improvements with symbolic regression and strong constraints on baryonic feedback,” *arXiv e-prints*, p. arXiv:2209.02075, Sep. 2022.
- [10] A. M. Delgado, D. Wadekar, B. Hadzhiyska, S. Bose, L. Hernquist, and S. Ho, “Modelling the galaxy-halo connection with machine learning,” *MNRAS*, vol. 515, no. 2, pp. 2733–2746, Sep. 2022.
- [11] F. Miniati and G. Gregori, “Learning transport processes with machine intelligence,” *Scientific Reports*, vol. 12, p. 11709, Jul. 2022.
- [12] W. La Cava, P. Orzechowski, B. Burlacu, F. Olivetti de França, M. Virgolin, Y. Jin, M. Kommenda, and J. H. Moore, “Contemporary Symbolic Regression Methods and their Relative Performance,” *arXiv e-prints*, p. arXiv:2107.14351, Jul. 2021.
- [13] M. Cranmer, A. Sanchez-Gonzalez, P. Battaglia, R. Xu, K. Cranmer, D. Spergel, and S. Ho, “Discovering symbolic models from deep learning with inductive biases,” *NeurIPS 2020*, 2020.
- [14] M. Cranmer, “Pysr: Fast & parallelized symbolic regression in python/julia,” Sep. 2020. [Online]. Available: <http://doi.org/10.5281/zenodo.4041459>



- [15] B. K. Petersen, M. Landajuela, T. N. Mundhenk, C. P. Santiago, S. K. Kim, and J. T. Kim, "Deep symbolic regression: Recovering mathematical expressions from data via risk-seeking policy gradients," *arXiv e-prints*, p. arXiv:1912.04871, Dec. 2019.
- [16] A. Meurer *et al.*, "SymPy: symbolic computing in python," *PeerJ Computer Science*, vol. 3, p. e103, Jan. 2017. [Online]. Available: <https://doi.org/10.7717/peerj-cs.103>
- [17] J. F. Navarro, C. S. Frenk, and S. D. M. White, "A Universal Density Profile from Hierarchical Clustering," *ApJ*, vol. 490, no. 2, pp. 493–508, Dec. 1997.
- [18] D. J. Bartlett, H. Desmond, and P. G. Ferreira, "Exhaustive symbolic regression function sets," Nov. 2022. [Online]. Available: <https://doi.org/10.5281/zenodo.7339113>
- [19] R. Andrae, T. Schulze-Hartung, and P. Melchior, "Dos and don'ts of reduced chi-squared," *arXiv e-prints*, p. arXiv:1012.3754, Dec. 2010.
- [20] J. Rissanen, "Modeling by shortest data description," *Automatica*, vol. 14, no. 5, pp. 465–471, 1978. [Online]. Available: <https://www.sciencedirect.com/science/article/pii/0005109878900055>
- [21] P. Grünwald and T. Roos, "Minimum Description Length Revisited," *arXiv e-prints*, p. arXiv:1908.08484, Aug. 2019.
- [22] P. Grünwald, *The Minimum Description Length Principle*. MIT Press, 2007.
- [23] A. D. Lanterman, "Schwarz, wallace, and rissanen: Intertwining themes in theories of model selection," *International Statistical Review*, vol. 69, no. 2, pp. 185–212, 2001. [Online]. Available: <https://onlinelibrary.wiley.com/doi/abs/10.1111/j.1751-5823.2001.tb00456.x>
- [24] T. M. Cover and J. A. Thomas, *Elements of Information Theory*, 2nd ed. Wiley, 1991.
- [25] J. Rissanen, "A Universal Prior for Integers and Estimation by Minimum Description Length," *The Annals of Statistics*, vol. 11, no. 2, pp. 416 – 431, 1983. [Online]. Available: <https://doi.org/10.1214/aos/1176346150>
- [26] C. S. Wallace and D. M. Boulton, "An Information Measure for Classification," *The Computer Journal*, vol. 11, no. 2, pp. 185–194, 08 1968. [Online]. Available: <https://doi.org/10.1093/comjnl/11.2.185>
- [27] C. Bogdanos and S. Nesseris, "Genetic algorithms and supernovae type Ia analysis," *J. Cosmology Astropart. Phys.*, vol. 2009, no. 5, p. 006, May 2009.
- [28] S. Nesseris and A. Shafieloo, "A model-independent null test on the cosmological constant," *MNRAS*, vol. 408, no. 3, pp. 1879–1885, Nov. 2010.
- [29] S. Nesseris and J. García-Bellido, "A new perspective on dark energy modeling via genetic algorithms," *J. Cosmology Astropart. Phys.*, vol. 2012, no. 11, p. 033, Nov. 2012.
- [30] D. Sapone, E. Majerotto, and S. Nesseris, "Curvature versus distances: Testing the FLRW cosmology," *Phys. Rev. D*, vol. 90, no. 2, p. 023012, Jul. 2014.
- [31] R. Arjona, "Machine learning meets the redshift evolution of the CMB temperature," *J. Cosmology Astropart. Phys.*, vol. 2020, no. 8, p. 009, Aug. 2020.
- [32] R. Arjona and S. Nesseris, "What can machine learning tell us about the background expansion of the Universe?" *Phys. Rev. D*, vol. 101, no. 12, p. 123525, Jun. 2020.
- [33] —, "Hints of dark energy anisotropic stress using machine learning," *J. Cosmology Astropart. Phys.*, vol. 2020, no. 11, p. 042, Nov. 2020.
- [34] G. Alestas, L. Kazantzidis, and S. Nesseris, "Machine learning constraints on deviations from general relativity from the large scale structure of the Universe," *arXiv e-prints*, p. arXiv:2209.12799, Sep. 2022.
- [35] R. Jimenez and A. Loeb, "Constraining Cosmological Parameters Based on Relative Galaxy Ages," *ApJ*, vol. 573, no. 1, pp. 37–42, Jul. 2002.
- [36] M. Moresco, "Raising the bar: new constraints on the Hubble parameter with cosmic chronometers at  $z \sim 2$ ," *MNRAS*, vol. 450, pp. L16–L20, Jun. 2015.
- [37] M. Moresco, L. Pozzetti, A. Cimatti, R. Jimenez, C. Maraston, L. Verde, D. Thomas, A. Citro, R. Tojeiro, and D. Wilkinson, "A 6% measurement of the Hubble parameter at  $z=0.45$ : direct evidence of the epoch of cosmic re-acceleration," *J. Cosmology Astropart. Phys.*, vol. 2016, no. 5, p. 014, May 2016.
- [38] A. L. Ratsimbazafy, S. I. Loubser, S. M. Crawford, C. M. Cress, B. A. Bassett, R. C. Nichol, and P. Väisänen, "Age-dating luminous red galaxies observed with the Southern African Large Telescope," *MNRAS*, vol. 467, no. 3, pp. 3239–3254, May 2017.
- [39] D. Stern, R. Jimenez, L. Verde, M. Kamionkowski, and S. A. Stanford, "Cosmic chronometers: constraining the equation of state of dark energy. I:  $H(z)$  measurements," *J. Cosmology Astropart. Phys.*, vol. 2010, no. 2, p. 008, Feb. 2010.
- [40] J. Simon, L. Verde, and R. Jimenez, "Constraints on the redshift dependence of the dark energy potential," *Phys. Rev. D*, vol. 71, no. 12, p. 123001, Jun. 2005.
- [41] N. Borghi, M. Moresco, and A. Cimatti, "Toward a Better Understanding of Cosmic Chronometers: A New Measurement of  $H(z)$  at  $z \sim 0.7$ ," *ApJ*, vol. 928, no. 1, p. L4, Mar. 2022.
- [42] C. Zhang, H. Zhang, S. Yuan, S. Liu, T.-J. Zhang, and Y.-C. Sun, "Four new observational  $H(z)$  data from luminous red galaxies in the Sloan Digital Sky Survey data release seven," *Research in Astronomy and Astrophysics*, vol. 14, no. 10, pp. 1221–1233, Oct. 2014.
- [43] M. Moresco *et al.*, "Improved constraints on the expansion rate of the Universe up to  $z \sim 1.1$  from the spectroscopic evolution of cosmic chronometers," *J. Cosmology Astropart. Phys.*, vol. 2012, no. 8, p. 006, Aug. 2012.
- [44] —, "Unveiling the Universe with Emerging Cosmological Probes," *arXiv e-prints*, p. arXiv:2201.07241, Jan. 2022.
- [45] M. Moresco, R. Jimenez, L. Verde, A. Cimatti, and L. Pozzetti, "Setting the Stage for Cosmic Chronometers. II. Impact of Stellar Population Synthesis Models Systematics and Full Covariance Matrix," *ApJ*, vol. 898, no. 1, p. 82, Jul. 2020.
- [46] A. G. Riess *et al.*, "Observational Evidence from Supernovae for an Accelerating Universe and a Cosmological Constant," *AJ*, vol. 116, no. 3, pp. 1009–1038, Sep. 1998.
- [47] S. Perlmutter *et al.*, "Measurements of  $\Omega$  and  $\Lambda$  from 42 High-Redshift Supernovae," *ApJ*, vol. 517, no. 2, pp. 565–586, Jun. 1999.
- [48] R. Tripp, "A two-parameter luminosity correction for Type Ia supernovae," *A&A*, vol. 331, pp. 815–820, Mar. 1998.
- [49] R. Kessler and D. Scolnic, "Correcting Type Ia Supernova Distances for Selection Biases and Contamination in Photometrically Identified Samples," *ApJ*, vol. 836, no. 1, p. 56, Feb. 2017.
- [50] D. Scolnic *et al.*, "The Pantheon+ Analysis: The Full Dataset and Light-Curve Release," *arXiv e-prints*, p. arXiv:2112.03863, Dec. 2021.
- [51] A. G. Riess *et al.*, "A Comprehensive Measurement of the Local Value of the Hubble Constant with  $1 \text{ km s}^{-1} \text{ Mpc}^{-1}$  Uncertainty from the Hubble Space Telescope and the SH0ES Team," *ApJ*, vol. 934, no. 1, p. L7, Jul. 2022.
- [52] D. Brout *et al.*, "The Pantheon+ Analysis: Cosmological Constraints," *arXiv e-prints*, p. arXiv:2202.04077, Feb. 2022.
- [53] P. Collaboration, "Planck 2018 results. VI. Cosmological parameters," *A&A*, vol. 641, p. A6, Sep. 2020.
- [54] T. A. Collaboration, "The Astropy Project: Building an Open-science Project and Status of the v2.0 Core Package," *AJ*, vol. 156, p. 123, Sep. 2018.
- [55] J. D. Hunter, "Matplotlib: A 2d graphics environment," *Computing in Science & Engineering*, vol. 9, no. 3, pp. 90–95, 2007.
- [56] L. Dalcin and Y.-L. L. Fang, "mpi4py: Status update after 12 years of development," *Computing in Science & Engineering*, vol. 23, no. 4, pp. 47–54, 2021.
- [57] F. Johansson *et al.*, *mpmath: a Python library for arbitrary-precision floating-point arithmetic (version 0.18)*, December 2013, <http://mpmath.org/>.
- [58] A. A. Hagberg, D. A. Schult, and P. J. Swart, "Exploring network structure, dynamics, and function using networkx," in *Proceedings of the 7th Python in Science Conference*, G. Varoquaux, T. Vaught, and J. Millman, Eds., Pasadena, CA USA, 2008, pp. 11 – 15.
- [59] P. A. Brodtkorb and J. D'Errico, "numdifftools 0.9.11," <https://github.com/pbrod/numdifftools>, Aug. 2015.
- [60] C. R. Harris *et al.*, "Array programming with NumPy," *Nature*, vol. 585, no. 7825, pp. 357–362, Sep. 2020. [Online]. Available: <https://doi.org/10.1038/s41586-020-2649-2>
- [61] T. pandas development team, "pandas-dev/pandas: Pandas," Feb. 2020. [Online]. Available: <https://doi.org/10.5281/zenodo.3509134>
- [62] Wes McKinney, "Data Structures for Statistical Computing in Python," in *Proceedings of the 9th Python in Science Conference*, Stéfan van der Walt and Jarrod Millman, Eds., 2010, pp. 56 – 61.
- [63] P. Virtanen *et al.*, "SciPy 1.0: Fundamental Algorithms for Scientific Computing in Python," *Nature Methods*, vol. 17, pp. 261–272, 2020.